Journal of Quantitative Spectroscopy & Radiative Transfer 326 (2024) 109108

Contents lists available at ScienceDirect

Journal of Quantitative Spectroscopy and Radiative Transfer

journal homepage: www.elsevier.com/locate/jqsrt

# On the retrieval of cloud optical thickness from spectral radiances - A sensitivity study with high albedo surfaces

Filippo Calì Quaglia [a,b,*], Giovanni Muscari [b], Daniela Meloni [c], Annalisa Di Bernardino [d], Tatiana Di Iorio [c], Giandomenico Pace [c], Sebastian K. Schmidt [e], Alcide di Sarra [f]

[a] DAIS, Ca' Foscari University of Venice, Venezia-Mestre 30172, Italy
[b] Istituto Nazionale di Geofisica e Vulcanologia, Rome 00143, Italy
[c] Laboratory for Observations and Measurements for Environment and Climate, ENEA, Rome 00123, Italy
[d] Department of Physics, Sapienza University of Rome, 00184 Rome, Italy
[e] Laboratory for Atmospheric and Space Physics, University of Colorado, Boulder, Co 80303, USA
[f] Laboratory for Observations and Measurements for Environment and Climate, ENEA, Frascati 00044, Italy

ARTICLE INFO

*Keywords:*
Cloud optical thickness
Thule High Arctic Atmospheric Observatory
Zenith radiance
UV-Vis-NIR spectra
libRadtran RTM

ABSTRACT

Measurements of spectral zenith radiance in the 320–950 nm wavelength range have been carried out since 2021 at the Thule High Arctic Atmospheric Observatory (THAAO, https://www.thuleatmos-it.it/, 76.5° N, 68.8° W, 225 m a.s.l) located in Pituffik, northern Greenland. This study evaluates whether such observations could provide, in principle, scientifically meaningful cloud optical depth (τ) estimates, what would be the limitations, which are the necessary auxiliary measurements, and which radiance wavelengths would be better suited for the goal. Although clouds play a critical role in the Arctic, a climatology of τ in high albedo conditions is particularly difficult to obtain. THAAO might have the instrument capabilities to provide such a long-term dataset. We use a radiative transfer package to simulate visible spectra with different cloud and surface conditions, assuming homogeneous overcast sky and liquid water clouds of fixed geometrical thickness. Simulations are run to reproduce typical conditions encountered at THAAO when measurements are carried out. We find that the assumption of a broadband albedo instead of a spectrally-resolved one is the source of the largest uncertainties. Tests on size and phase of cloud particles showed that a 50% uncertainty in $r_{eff}$ leads to a ~10% error in τ, and that a 10% contamination of ice crystals in a low-level liquid water cloud leads to an error in τ estimates of less than 5%. All the tests showed that the most critical τ range is between the thin and thick cloud regimes (τ ~ 7–15), where the retrievals can be less reliable. Otherwise, tests suggest that in the environmental conditions that characterize late spring and summer at THAAO, and given the observatory measurements capabilities, estimates of τ for low-level clouds could be accurately retrieved both in high and low surface albedo conditions by means of zenith radiance measurements in the UV-Vis-NIR range.

## 1. Introduction

The Arctic is a complex environment strongly affected by climate change. It is characterized by poor accessibility, scarcity of measurements and harsh environmental conditions. The most recent analyses for this area point towards an increase in surface temperature four times greater than the global average during the last 70 years [6,50]. This phenomenon, referred to as Arctic Amplification, has been studied to better understand the processes involved and their mutual feedback. In this framework, clouds are of utmost importance. Their effects on downwelling and upwelling radiation are complex and have been extensively studied (e.g., [9,19,22,60]). Moreover, clouds and radiation interact with other sensitive components of the Arctic climate system, such as aerosol, both natural and anthropogenic [49,57], sea ice [14], and continental glaciers [4].

Understanding the critical role that clouds play in the Arctic climate has been among the primary scientific objectives of large recent international experiments such as the *Multidisciplinary drifting Observatory for the Study of Arctic Climate (MOSAiC)* [54], the *World Meteorological Organisation (WMO) Polar Prediction Project* [29], and the *Arctic Amplification: Climate relevant Atmospheric and Surface Processes and Feedback Mechanisms*, ((AC)3 campaign, [61]), among others, as well as the main

* Corresponding author.
*E-mail addresses:* filippo.caliquaglia@ingv.it, filippo.caliquaglia@unive.it (F. Calì Quaglia).

https://doi.org/10.1016/j.jqsrt.2024.109108
Received 22 May 2023; Received in revised form 26 June 2024; Accepted 29 June 2024
Available online 30 June 2024

topic of the current *NASA Arctic Radiation-Cloud-Aerosol-Surface Interaction Experiment* (ARCSIX, [51]).

The main cloud properties determining impact on solar and infrared radiation are related to their composition and structure, i.e., the cloud optical thickness ($\tau$), the droplet effective radius ($r_{eff}$), the cloud geometrical thickness ($z_c$), the cloud base height ($h_{cb}$), the thermodynamic phase ($\phi$; liquid, ice, or mixed-phase), the shape of ice crystals, and the vertical profile of these components. The knowledge of these parameters and their impact on radiation leads to improved calculations of the radiative budget in the Arctic, which is vital for a better understanding of how the changing climate will shape this region.

Among the various types of clouds, those containing liquid water play a major role in the Arctic [4]. [53] reports that liquid water clouds occur in 35–50% of cloud occurrences at two Arctic sites: Utqiaġvik, Alaska, USA, and Eureka, Nunavut, Canada. However, by using measurements from CALIOP and the infrared imaging radiometer (IIR) aboard CALIPSO, [28] pointed out that high-latitude, low-level stratus clouds (cloud base height lower than 2 km) with temperature above $-40^{\circ}$C are supercooled water clouds in 95% of cases.

A reliable climatology of cloud characteristics is difficult to obtain over polar regions. In snow-covered areas, the high surface albedo ($\gamma$) has a critical role since it determines an elevated amount of multiple scattering, making the retrieval of cloud characteristics from measurements of scattered radiation more challenging [23]. Furthermore, the spectral features of high-albedo surfaces are strongly different from those of vegetated surfaces and vary with the snow composition and characteristics [24], such as snow grain size or light-absorbing impurities. For this reason, in addition to geographical and technical limitations, NASA AERONET sites [25,27,56] do not provide regular, long-term $\tau$ estimates in the polar regions.

Several attempts were conducted to estimate $\tau$ and $r_{eff}$ from ground-based or airborne platforms. Methods for retrieving these quantities from satellite measurements were also proposed (e.g., [32,44,48,65]), but the information available from cloud top reflectivity mainly refers to the characteristics of the upper exposed layer. Conversely, transmissivity measured at the ground depends on radiation scattered through the cloud and shows non-monotonic shapes, increasing with increasing $\tau$ for thin clouds and then decreasing for $\tau$ values above a certain threshold (e.g., [11,12]). In early 2000, various authors proposed inversion methods to retrieve total cloud cover, $\tau$ and $r_{eff}$ from ground-based instruments (e.g., [10,31,36,37]). Leontyeva and Stamnes [35] first discussed the use of irradiance measurements for estimating $\tau$. Irradiance measurements were also exploited by Min and Harrison [43], by means of a ground Multi-Filter Rotating Shadowband Radiometer (MFRSR), and by Barnard and Long [2] and Barnard et al. [1] In particular, Barnard and Long [2] showed that $\tau$ can be obtained from irradiance measurements but some limiting assumptions are necessary: 1) there must be an 8 oktas cloud cover, 2) $r_{eff}$ must be assumed as $\tau$ and $r_{eff}$ cannot be concurrently retrieved, 3) albedo conditions are restricted to $\gamma < 0.3$, and 4) high solar zenith angles cannot be considered. A different approach consists of using liquid water path (LWP) measurements to retrieve $\tau$ using the formulas derived from the assumption on the extinction efficiency coefficient for liquid water spherical droplets [15,62]. These methods can provide estimates affected by the uncertainty on the LWP measurements, usually performed via microwave radiometers, which can reach 20 g/m$^2$. Moreover, also these techniques require assumptions on the homogeneity of cloud cover and $r_{eff}$. Other attempts have been conducted by Chiu et al. [12], exploiting solar background radiation collected by ceilometers and reaching an overall retrieval uncertainty of about 10%. A "bi-spectral" approach, which exploits the information contained in the radiance at the zenith for ground-based platforms at two different wavelengths, is also widely used to estimate $\tau$ and is described by Chiu et al. [10,11]. This method has been adopted for the NASA AERONET network, which is present worldwide with its Cimel sunphotometers. An important drawback of this method is that it is proven to work only in the presence of vegetated surfaces as it uses the sharp difference in albedo at the two wavelengths used (440 nm and 870 nm).

The simultaneous retrieval of $\tau$ and $r_{eff}$ can be achieved when spectral measurements of zenith radiances are available over a wider range of wavelengths (e.g., 300 to 2500 nm). In these cases, combinations of transmissivities at different wavelengths can be used to overcome the indetermination caused by the non-monotonic dependence of a single transmissivity on $\tau$ (e.g., [7,30,34,39,46,67]). Brückner et al. [7] used ratios between transmissivities at various wavelengths to discriminate between thin and thick cloud regimes. LeBlanc et al. [34] list 15 different band combinations of normalized radiances in the UV-Vis-NIR and SWIR and aim to fully retrieve optical and microphysical characteristics of clouds: $\phi$, $\tau$, and $r_{eff}$. Zinner et al. [67] calculate a slope with radiance values in the blue range of wavelengths. Niple et al. [45] and Zinner et al. [68] exploit the signal in the $O_2$-A band within the 755–775 nm wavelength range to obtain information on $\tau$ and cloud distance from the observer. A similar technique has also been applied to satellite retrievals over snow-covered surfaces by Zhou et al. [65]. It is worth pointing out that the information on $\tau$ and $r_{eff}$ is not uniformly contained in the two spectral ranges of 300–1000 nm (UV-Vis-NIR) and 1000–2500 nm (SWIR), which are typically covered by different detectors (Si and InGaAs photodiode arrays, respectively). The information on $\tau$ is prominent in the UV-Vis-NIR spectral region, while wavelengths in the SWIR range have been decisive in accessing the information on $r_{eff}$. The accurate analysis performed by Coddington et al. [13] quantifies the information content at different wavelengths.

This work is an assessment study on retrieving $\tau$ values by means of zenith radiance measurements in the wavelength range 320–950 nm. It does not validate a method to do so with actual measurements. We explore what conditions and ancillary measurements would be required in order to retrieve $\tau$ on a regular basis at the Thule High Arctic Atmospheric Observatory (THAAO, 76.5° N, 68.8° W, 225 m a.s.l.), located near the Pituffik Space Base (formerly known as Thule Air Base), Greenland. This article focuses on the case of high $\gamma$ surfaces, typical of polar regions, and on environmental conditions and instrument characteristics present at THAAO. We use a radiative transfer package to simulate transmittance spectra, allowing us to investigate the sensitivity of various combinations of transmittances to different cloud, atmospheric and surface conditions.

Section 2, Data and Methods, briefly introduces THAAO, illustrates the transmissivity combinations considered for the retrievals, and provides the details and settings of the radiative transfer model used. Section 3, Sensitivity study results, discusses the uncertainties related to different variables that need to be considered when performing the retrieval: $\gamma$, $\gamma_{SP}$, $\phi$, $h_{cb}$, and $r_{eff}$. Section 4, Summary and Conclusions, highlights the strengths and weaknesses of each spectral combination and the limits of using UV-Vis-NIR zenith radiances for estimating $\tau$.

## 2. Data and methods

### 2.1. The zenith-looking spectrometer and the additional ground-based instruments at Thaao

Measurements of zenith radiance ($L_\lambda$) with a TriOS RAMSES ARC-VIS zenith-looking spectrometer [66] have been carried out at THAAO during the sunlit portion of years 2022 and 2023. The RAMSES is an instrument consisting of a Monolithic Miniature Zeiss Spectrometer that covers the 320 - 950 nm wavelength range (UV-Vis-NIR). It has a spectral Full Width at Half Maximum (FWHM) of 10 nm and a pixel dispersion of 3.3 nm/pixel with 190 usable channels. The instrument's full-angle field of view is 7°. The maximum reported uncertainty for a single 10 μs measurement is 6%. These instrumental specifications have dictated specific settings of the radiative transfer model employed in this work. Concurrent data from other ground-based instruments are available at THAAO and are discussed here to justify the choices made on the settings of the radiative transfer model simulations. At THAAO, $h_{cb}$ can

**Table 1**
Summary of transmissivity formulas (TFs). $\mathbf{T_\lambda}$ is the transmissivity value calculated from $\mathbf{L_\lambda}$ (Eq. 1), $\boldsymbol{\delta_T}$ is the radiometric uncertainty propagated from radiance measurements following Eq. 1, $\boldsymbol{\delta_\lambda}$ is the assumed spectral resolution of radiance measurements, $\boldsymbol{\delta_{FWHM}}$ is their FWHM, and **SNR** is their signal-to-noise ratio. The equivalent width uncertainty formula is adopted from Cayrel de Strobel [8]. In the case of TF4, the formula has been modified from the algorithm in Zinner et al. [68]. See text for more details.

| TF name | Wavelengths [nm] | TF | Uncertainty | Reference |
|---|---|---|---|---|
| TF1 | 440 | $T_{440}$ | $\delta_T T_\lambda$ | / |
| TF2 | 870 | $T_{870}$ | $\delta_T T_\lambda$ | / |
| TF3 | 450, 680 | $T_{450}/T_{680}$ | $\sqrt{(\delta_T T_{450})^2 + (\delta_T T_{680})^2}$ | [7] |
| TF4 | 761, 775 | $T_{761}/T_{775}$ | $\sqrt{(\delta_T T_{761})^2 + (\delta_T T_{775})^2}$ | [68] |
| TF5 | 755–775 | $\int_{755}^{775} T_\lambda d\lambda$ | $\frac{3}{2}\frac{\sqrt{\delta_{FWHM}\delta_\lambda}}{SNR}$ | [45] |

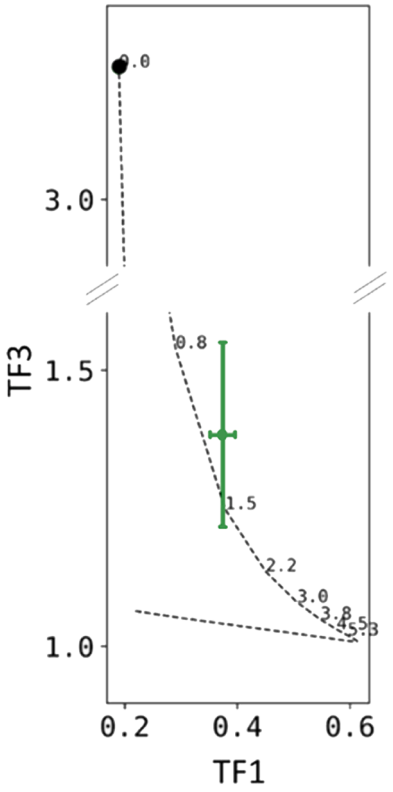


**Fig. 1.** A conceptual example of the τ retrieval procedure using the pair TF3 vs. TF1. The zenith radiance measurements (transformed in transmissivity and indicated with a green cross) were collected at THAAO on May 4, 2022. The measured TF pair is depicted in the figure with its uncertainties, calculated propagating the 6% uncertainty on the measured radiances. The simulations at varying τ (i.e., the 23 LWP steps) are drawn with a dashed curve, and the corresponding τ values are indicated in digits and shown only for the thin cloud regime. Clear sky conditions are indicated with a black solid circle. The modeled atmospheric and cloud conditions are specific to May 4, 2022 (θ=60°, γ=0.60, $h_{cb}$=0.5 km, $z_c$=500 m, and $r_{eff}$=10 μm).

be extracted from the measurements of a ceilometer (a Lufft CHM 15k Nimbus) operating at the wavelength of 1064 nm [18]. Downwelling and upwelling shortwave irradiance measurements by Eppley PSP and Kipp&Zonen CMP21 pyranometers, respectively [41,42], are conducted continuously at THAAO and can provide broadband albedo estimates [40]. More details on the general conditions at THAAO can be found on the website (https://www.thuleatmos-it.it) and in Di Biagio et al. [17].

For the model initialization, we also considered the data from a NASA AERONET Cimel installed on the roof of THAAO and the MERRA-2 (Modern Era-Retrospective Analysis for Research and Analysis) model.

### 2.2. Transmissivity formulas (TFs) considered

The simulated zenith radiances ($L_\lambda$) calculated using the libRadtran (v. 2.0.5; [20,38]) Radiative Transfer Model (RTM) were converted into transmissivities ($T_\lambda$; Eq. 1) using the extra-terrestrial spectrum (E0) by Kurucz [33] at 0.1 nm resolution:

$$T_\lambda = \frac{\pi L_\lambda}{E_0 \cos(\theta)} \quad (1)$$

Different combinations of transmissivities at different wavelengths were exploited to obtain an estimate of τ. Throughout this study, we use the term transmissivity formula (TF) for a transmissivity at a single wavelength (e.g., $T_{440}$) or for any formula that uses a combination of transmissivities (e.g., a ratio between two transmissivities). All the TFs considered in this study are listed in Table 1.

From left to right, the columns of Table 1 summarize for each TF the involved wavelengths, the applied formula to calculate TF, the formula used to calculate TF's uncertainty, and the reference publication where the same combination of transmittances was first employed. It is worth mentioning that the publications reported in Table 1 use different ancillary data and/or employ measurements over a wider spectral range with respect to the present study. TF1 and TF2 present the typical non-monotonic behavior. TF3 was originally used by the authors to discriminate between thick and thin clouds. In fact, in the presence of thin clouds, the scattering is larger at shorter wavelengths (i.e., $T_{450}$) if compared to longer wavelengths (i.e., $T_{680}$). Additionally, TF4 was modified with respect to the original ratio proposed by Zinner et al. [68], as here it is calculated as the ratio between the minimum of the absorption band of the $O_2$-A at 761 nm and the value on the spectral plateau at 775 nm. In the original work, it was used to estimate horizontal distance and vertical height of clouds measured from an aircraft. TF5 is based as well on the absorption in the $O_2$-A band, but is calculated as the integral of the transmittance over the band. We had initially considered two additional transmissivity combinations published in the literature, those by Zinner et al. [67] and LeBlanc et al. [34], but their combinations carried the same information content as TF3 [7], and they are not discussed in this study.

TF1, TF2, and TF3 display a non-monotonic dependency on τ (see Figures S1 and S2 in the supplementary material), with values changing rapidly for increasing τ (thin cloud regime), reaching a positive or negative peak and then inverting the trend for a further increasing τ (thick cloud regime). TF4 and TF5, both based on the $O_2$-A band transmissivity, show a nearly monotonic dependence with varying τ but, at the same time, appear to be less sensitive to τ variations.

Since no single TF displays both a monotonic behavior as a function of τ and a significant sensitivity to τ variations over a wide range of values (see Figures S1 and S2), in this feasibility study we paired TFs to separate thin and thick cloud regimes. For this study, one of the two TFs used in each pair shown is always TF1, but, in principle, other combinations can be used successfully. Curves obtained by varying τ on a TF vs. TF plane are presented in Figs. 2 and 3 and discussed in Section 3.

### 2.3. Model details

This study uses the libRadtran RTM package. It employs the DIScrete Ordinate Radiative Transfer solver (DISORT; [55]) with 16 streams, the pseudospherical approximation [16], unpolarised radiation, Mie pre-calculated tables for scattering phase function and the representative wavelength approach (REPTRAN) at coarse resolution. The model settings were chosen to reproduce environmental conditions consistent with the location of THAAO. The zenith radiance spectra modeled for a single specific condition of θ, γ, $h_{cb}$, $z_c$, $r_{eff}$, ϕ, and liquid water content

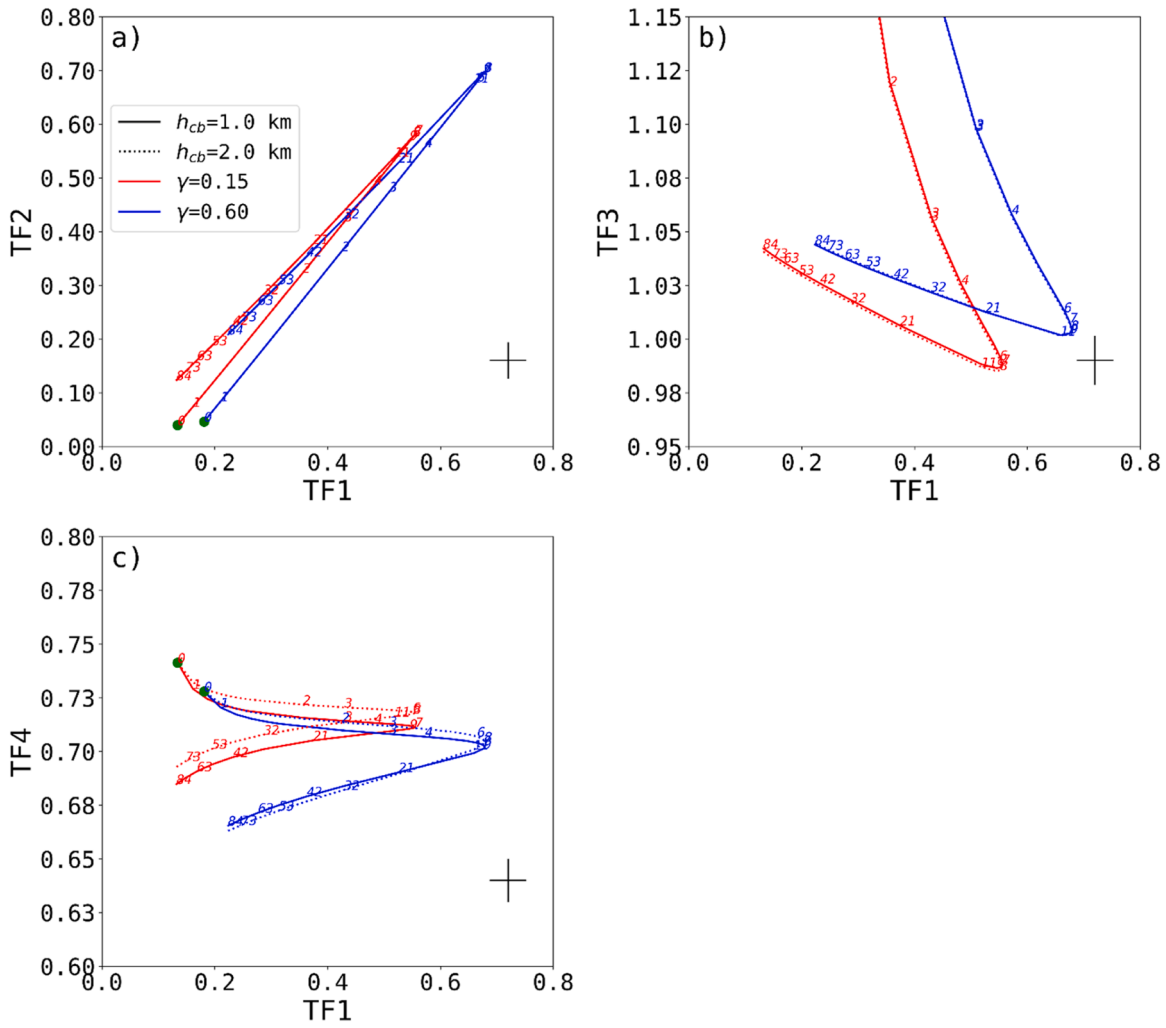


**Fig. 2.** Plots of different TFs versus TF1 for γ=0.15 (in red) and 0.60 (in blue), for $h_{cb}$=1.0 km (solid lines) and 2.0 km (dotted lines), θ=52° and $r_{eff}$=9 μm. τ is indicated in rounded values in each panel. Green dots (•) indicate τ=0 (clear sky). The cross in the bottom right corner of each graph shows the maximum uncertainty values on the corresponding TFs. They are calculated using the propagation formulas of Table 1, assuming a 6% maximum uncertainty on the radiance measurements. See text for further details.

(LWC) are used as synthetic measurements and the corresponding cloud optical thickness is indicated with $\tau_{true}$. It is assumed that LWC does not vary within the cloud, and LWP = $z_c$ * LWC, with $z_c$ held constant at 500 m throughout this study.

*Atmospheric profiles and components*. The "subarctic summer" pressure, temperature, humidity and trace gases vertical profiles provided within the RTM were used. The default aerosol type for the model is used [52], consisting of a rural type aerosol in the boundary layer, background aerosol above 2 km, spring-summer conditions, and a visibility of 50 km. The tropospheric aerosols below 2 km (*aerosol_haze=6*) are vertically distributed according to the model summer-spring profile (*aerosol_season=1*) and rescaled to an aerosol optical depth of 0.06, representing the annual average measured by the NASA AERONET instrument installed at THAAO. The model was set with a precipitable water vapor of 6 mm (annual average measured by the NASA AERONET instrument installed at THAAO). Total ozone and surface pressure settings were obtained from the annual averages calculated by the MERRA-2 model and were set at 338 DU and 985 hPa, respectively.

*Surface albedo (γ)*. The calculations used two different surface broadband albedo values, corresponding to values measured at THAAO during different times of the year [40]: γ=0.15 for bare ground and γ=0.60 typical of snow-covered ground at THAAO, with a broadband albedo uncertainty of 0.02 assumed based on measurements at THAAO. Additional simulations were performed with γ=0.58 and γ=$\gamma_{SP}$, where $\gamma_{SP}$ is a spectral albedo chosen among those listed in the ECOSTRESS Spectral Library (https://speclib.jpl.nasa.gov/). These additional simulations were conducted to evaluate the sensitivity of the retrievals to albedo uncertainties and constraints. Specifically, as spectral albedo we used the “Coarse Granular Snow” type and rescaled it for the spectral irradiance at the surface over the 0.3–2.8 μm interval to match the broadband value of 0.60. The albedo of surfaces covered by snow or ice generally displays a reasonably flat spectral behavior, with high values slightly decreasing for λ>700 nm.

*Clouds ($r_{eff}$, $h_{cb}$, $z_c$, ϕ)*. We assumed a homogeneous single-layer low-level liquid cloud with 8 oktas of cloud cover at two $h_{cb}$ values (1.0 or 2.0 km) and a fixed cloud geometrical thickness ($z_c$=500 m). In general, however, Arctic stratus clouds at 1 or 2 km altitude in late spring and summer are largely, when not entirely, made of liquid droplets (e.g., [28]). Simulations of liquid water clouds were run with LWP values ranging from 0.0 (clear sky) to 500 g/m$^2$ at 23 steps, which were not uniformly distributed. LWP values were converted into τ according to the relation τ = (3 * $z_c$ * LWC) / (2 * $r_{eff}$) = (3 * LWP) / (2 * $r_{eff}$). Since no direct measurement of $r_{eff}$ is currently available at THAAO, we performed the simulations with $r_{eff}$ values that are close to those found in the literature for liquid-bearing clouds in the Arctic region. Yin and Min [64] presented an interesting dataset for Utqiaġvik (formerly known as

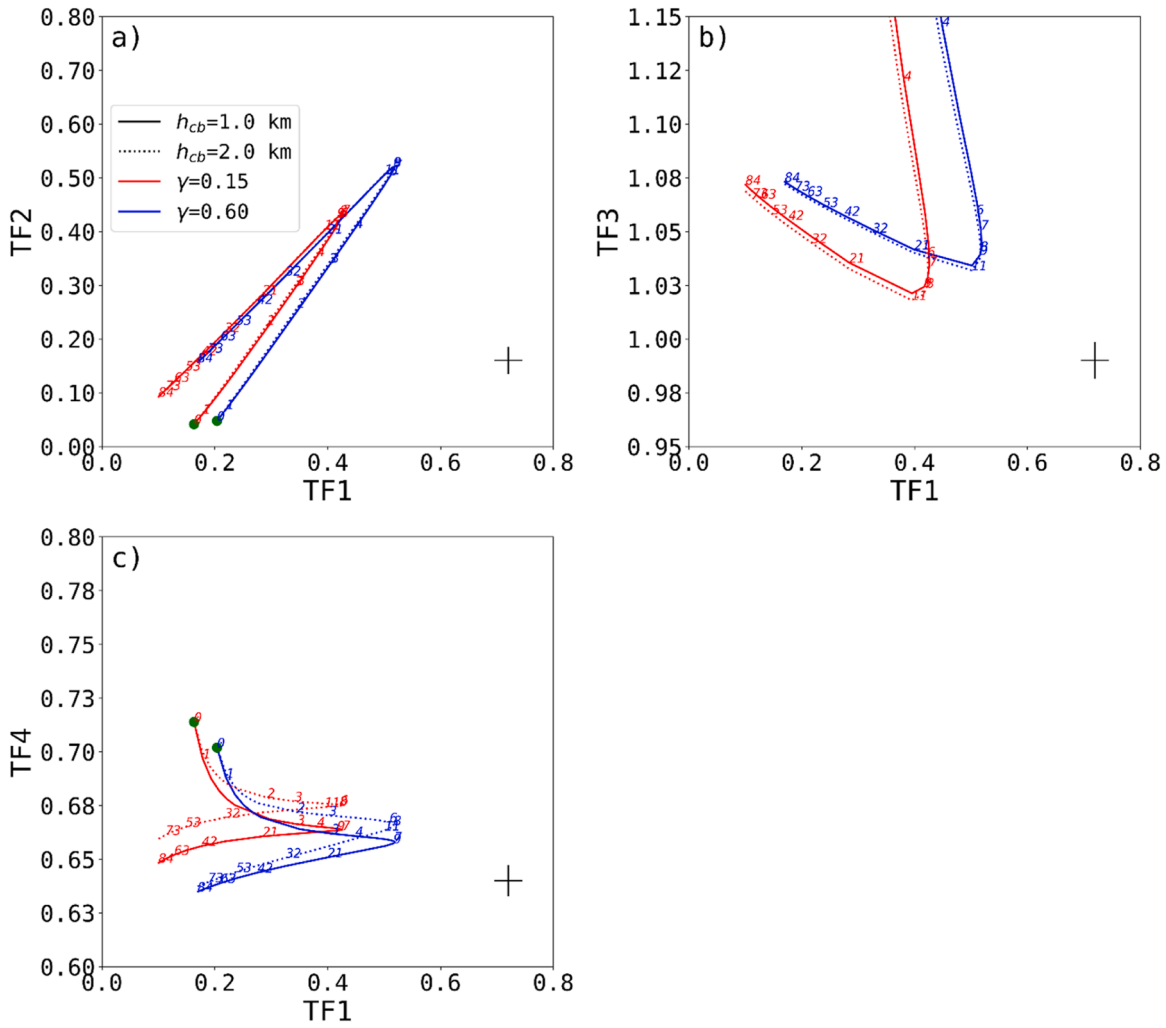


**Fig. 3.** Same as Fig. 2 but for θ=70°.

Barrow, 71.3°N, 156.8°W), where the climatological seasonal variability of $r_{eff}$ is comprised between 10 and 12 μm. Other studies in the Arctic region [5,47] suggest similar values. Therefore, we ran the simulations for three different values of $r_{eff}$: 6, 9, and 12 μm. The combination of this set of parameters leads to a minimum $\tau > 0$ of 0.12 for LWP=1 g/m$^2$ and $r_{eff}$=12 μm, and a maximum τ of 125 for LWP=500 g/m$^2$ and $r_{eff}$=6 μm.

In order to evaluate the potential radiative impact of ice crystals instead of liquid droplets, a test with an ice cloud was also conducted. In this case, atmospheric variables were set to θ=70°, $r_{eff}$=20 μm, IWP = $z_c$ * IWC (Ice Water Content) values ranging from 0.0 (clear sky) to 500 g/m$^2$ at 23 steps (with τ=0.08 at the first step of IWP=1 g/m$^2$), $z_c$=500 m, γ=0.60, $h_{cb}$=1.0 km. τ values were extracted from the libRadtran model calculations.

*Solar Zenith Angle (θ).* We ran simulations for θ=52° and 70°. θ=52° represents the lowest θ for the THAAO location, while θ=70° is representative of the local average condition.

*Radiance spectral uncertainty.* Simulated spectra obtained with the RTM have a higher spectral resolution with respect to the RAMSES radiance measurements. In order to match the resolution of the measurements, the modeled spectra are convolved using a Gaussian slit function. The overall uncertainty of synthetic radiance measurements was set to 6% to match the accuracy of the RAMSES measurements. The FWHM ($\delta_{FWHM}$) of spectral channels is set at 10 nm and the pixel dispersion ($\delta_\lambda$) is 3.3 nm/pixel.

### 2.4. τ retrievals based on TF pairs: an example using Ramses trios radiance measurements

This paragraph shows how the τ retrieval procedure works when using a pair of TFs applied to actual zenith radiance measurements (transformed in transmissivity and indicated with the green cross in Fig. 1) collected at THAAO on May 4, 2022.

Our aim with this example is to show the τ retrieval procedure using two TFs, in particular TF3 and TF1. Measurements are depicted in Fig. 1 with their uncertainties, which can be seen as the axes of an ellipsis. Uncertainties are calculated by propagating the 6% maximum uncertainty on the measured zenith radiances using the formulas indicated in Table 1 for TF1 and TF3. The simulations at varying τ (i.e., different LWP) are drawn with a dashed curve, and the corresponding τ values are indicated in digits and shown only for the thin cloud regime. In this libRadtran simulation, θ=60°, γ=0.60, $h_{cb}$=0.5 km, $z_c$=500 m, and $r_{eff}$=10 μm. Clear sky conditions are indicated with a solid black circle. For every spectral measurement, the retrieval is successful only when the ellipsis of the error of the TFs overlaps with the modeled curve. The retrieved value of τ corresponds to the point of the modeled curve that is the closest to the measurement. In Fig. 1, the retrieval succeeds and indicates a τ=1.2.

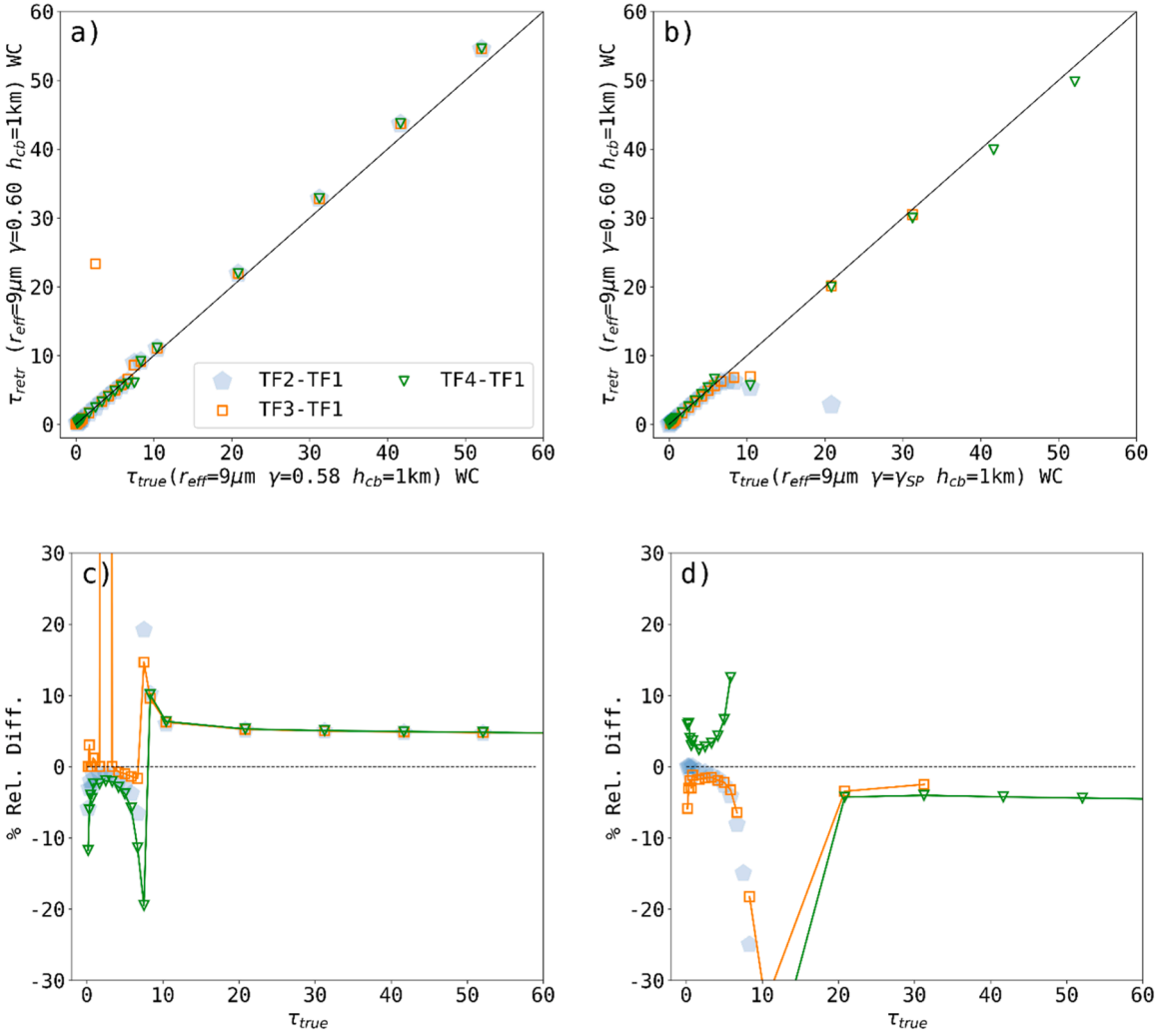


**Fig. 4.** Scatterplot showing $\tau_{true}$ and $\tau_{retr}$ for each pair of TFs in the case of modeled radiances of liquid water clouds (WC) with a) $\gamma$=0.58 and b) $\gamma=\gamma_{SP}$. Panels c and d show the relative difference 100 * ($\tau_{retr}$ - $\tau_{true}$) / $\tau_{true}$ for the cases displayed in a and b, respectively.

## 3. Sensitivity study results

### 3.1. Sensitivity of TF pairs to surface $\gamma$, $h_{cb}$ and $\theta$

Fig. 2 shows modeling results for different pairs of TFs using two values of surface albedo, $\gamma$=0.15 (in red) and $\gamma$=0.60 (in blue), two values of cloud base height, $h_{cb}$=1.0 km (solid line) and 2.0 km (dashed line), $r_{eff}$=9 μm, and $\theta$=52° Results for the same conditions but $\theta$=70° are displayed in Fig. 3. Numbers along the curves represent rounded $\tau$ values. The uncertainty in determining TFs values plays a key role in the success of the retrieval method. The 6% maximum uncertainty on the radiances is propagated (see Table 1) to estimate the impact of such uncertainty on the TFs. Error bars referring to the maximum uncertainties for each TF are depicted in each panel. When calculating these uncertainties, it appeared that the uncertainty of TF5 was extremely large and prevented any possibility of estimating $\tau$ with sufficient accuracy. Therefore, we removed TF5 from the set of algorithms shown in Figs. 2 and 3, and it will not be discussed any further. It is interesting to note that the uncertainty on TF5 is the only one that is based only on the instrumental characteristics. The availability of more accurate radiance measurements would allow a re-evaluation of this TF.

TF3 vs. TF1 in Fig. 2b shows a useful separation between the two branches representing thin and thick clouds and a maximum uncertainty of both TFs that would allow the identification of the cloud regime. This pair also does not depend significantly on $h_{cb}$, with solid and dashed lines almost exactly superimposed. In the thick cloud regime, TF1 is more sensitive to $\tau$ with respect to TF3, which is characterized by small changes when $\tau$ increases significantly. Fig. 2a shows the TF2 vs. TF1 pair which exhibits a strong overlap between the thin and thick cloud regimes. In order to use this pair to estimate $\tau$ by means of RAMSES radiances, information on the cloud regime must be obtained with auxiliary measurements. The valuable aspects of this pair are the little sensitivity to $h_{cb}$ and the small TF uncertainties estimated. For the TF4 vs. TF1 pair in Fig. 2c, the high albedo case shows a significant separation between the two cloud regimes, which, however, in the low albedo case becomes too small for most $\tau$'s. This pair shows a larger separation between the blue and red curves in the thick cloud regime, starting from $\tau$ larger than ~6–8, compared to the other two pairs. In general, however, it appears that an accurate estimate of the surface albedo is important. In most cases, the separation between the curves with different albedos (blue and red curves) is limited and this implies that a radiance spectral measurement drawn in the TFx vs. TF1 chart could lie close to very different $\tau$ values belonging to different albedo curves. The broadband albedo measurements carried out at THAAO are, therefore, a key ingredient for estimating $\tau$.

The impact of increased $\theta$ values on the set of TFs correlation curves can be noted by comparing Figs. 2 and 3. With a larger solar zenith angle, all pairs show a larger separation between the thin and thick cloud regimes. Additionally, with a larger $\theta$, the dependence on $h_{cb}$ increases and the dashed curves in Fig. 3 move away from the solid ones.

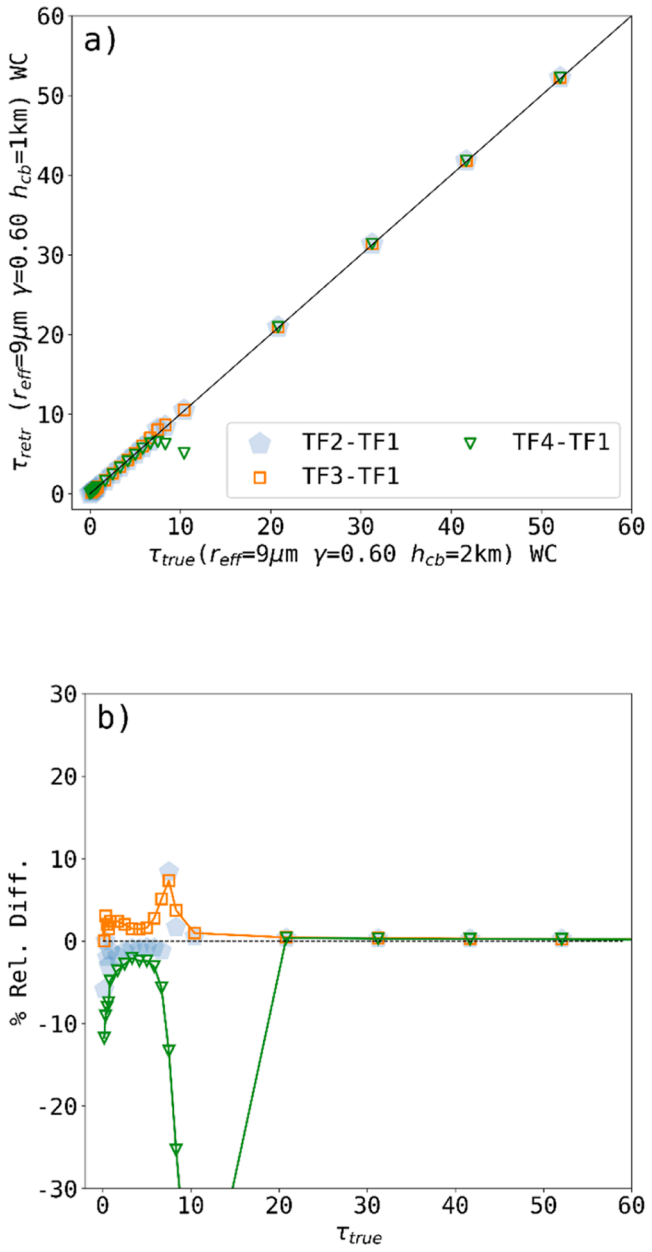


**Fig. 5.** Same as Fig. 4 but using modeled radiances with γ=0.60 and $h_{cb}$=2.0 km.

### 3.2. Retrieval sensitivity to surface albedo (γ and $\gamma_{SP}$), $h_{cb}$, $r_{eff}$ and cloud thermodynamic phase (ϕ)

Additional simulations were conducted to estimate the impact on the retrieval of τ due to: 1) the uncertainty on the broadband albedo measurements carried out at THAAO (0.02), 2) the use of broadband albedo values instead of spectrally-resolved values, 3) a large error on the cloud base height (1.0 km), 4) the use of an annual and regional average value for $r_{eff}$ instead of an actual measurement, and 5) an erroneous assumption on the liquid phase of the cloud. As discussed in Section 2.3, we use the libRadtran RTM to produce zenith radiance spectra at set values of θ, γ, $h_{cb}$, $z_c$, $r_{eff}$, ϕ and with LWP (or IWP for ice clouds) varying in 23 steps from 0 to 500 g/m$^2$, producing an associated set of clouds with varying τ values. As discussed above, the default values of the above parameters are ϕ=water, θ=70°, γ=0.60, $h_{cb}$=1.0 km, $z_c$=500 m, and $r_{eff}$=9 μm. We tested the impact of each parameter on the retrieved value of τ by generating modeled zenith radiances (with associated τ values) having one of the parameters varied with respect to its default value and holding all the other parameters at their default values. This state was assumed to represent the "true" atmosphere and the corresponding τ is indicated as $\tau_{true}$. We then performed the retrieval of τ ($\tau_{retr}$) with the TF pairs built by using the default values, which, therefore, differ from the true state of the atmosphere by only one parameter. The retrieved $\tau_{retr}$ is compared with $\tau_{true}$, showing the deviation of our estimate of τ from its true value.

A first parameter, the surface albedo, is discussed in Fig. 4, which summarizes the impact on estimating τ when the modeled radiances are produced using γ=0.58 (Fig. 4a, c) or γ=$\gamma_{SP}$ (Fig. 4b, d) and the retrieval assumes instead the default value of γ=0.60.

The impact of a 0.02 error (the estimated uncertainty) on the broadband surface albedo value varies depending on the cloud regime (Fig. 4a, c). For τ<7, $\tau_{retr}$ values obtained with the TF3-TF1 pair are the closest to $\tau_{true}$ (except for one outlier), with the other two pairs displaying a small underestimation of less than 5% throughout most of the thin clouds range (Fig. 4c). For τ>10, $\tau_{retr}$ obtained with any of the discussed algorithms overestimates $\tau_{true}$ by approximately 8%. The worst results are obtained for $\tau_{true}$ values between 7 and 10 at the transition from thin to thick cloud regimes, where the two regime branches are close to one another (Figs. 2 and 3) and the retrievals can be less reliable. When a spectrally-resolved albedo γ=$\gamma_{SP}$ is used to model the true atmosphere (Fig. 4b, d), some critical issues arise if we derive τ using the default value of broadband albedo γ=0.6 instead. As mentioned earlier, for the spectrally-resolved albedo the "Coarse Granular Snow" type from libRadtran was used and rescaled to match the broadband value of 0.6. For $\tau_{true}$<8, all TF pairs succeed in the retrievals with TF2 and TF3 vs. TF1 showing slightly better results. Here again, there is a range between the two cloud regimes (in this case, approximately between 8 and 18) where all the TF pairs appear to be less reliable. Retrievals using the TF2-TF1 pair are unreliable for $\tau_{true}$>10 and fail above 20. For $\tau_{true}$ between 20 and 30 both TF3 and TF4 vs. TF1 provide quite accurate estimates of τ, with an underestimation of less than 5%, but then for $\tau_{true}$>30, only the TF pair based on the $O_2$-A band (TF4 vs. TF1) succeeds, showing a weak underestimation (~%5). This is an important result of this study, as it reveals that out of the several potential transmittance formulas that were considered if ancillary information on the spectral albedo is not available only TF4 can handle large τ values.

The sensitivity study on a second parameter, the cloud base height, $h_{cb}$, is shown in Fig. 5. Here the impact on $\tau_{retr}$ using modeled radiances with $h_{cb}$=2.0 km is summarized. The pair TF4 vs. TF1 is the one that shows problems in case of large uncertainties on $h_{cb}$ but only for values of $\tau_{true}$ between approximately 8 and 18, just as in the previous test and for the same reason of having the two regime branches very close to one another (see Figs. 2 and 3). The other two pairs of TFs do not appear to be strongly affected by assuming a significant wrong cloud base height in the retrieval.

Fig. 6 summarizes the impact on each retrieval when the "true" atmosphere has a cloud with $r_{eff}$=6 μm or $r_{eff}$=12 μm and in the retrieval of τ we assume $r_{eff}$=9 μm. For τ>10, using a $r_{eff}$ of 9 μm in the retrieval instead of the 6 μm of the "true" cloud (Fig. 6a, c) leads to a τ overestimation of 10%. In the same τ range, our assumption of a $r_{eff}$=9 μm in the retrieval when the "true" cloud is made of 12 μm droplets (Fig. 6b, d) leads to an underestimation of 5%. It must be noted that the relative error in $r_{eff}$ (25–50%) is much larger than the corresponding relative bias on τ (5–10%). For τ<10 results are more variable but remain within a satisfactory relative error, with the TF3 vs. TF1 pair showing slightly larger biases with respect to the other two pairs. The 6 and 12 μm $r_{eff}$ values were chosen for the test as they represent the most likely interval of $r_{eff}$ to be found in Arctic low-level water clouds [58,64].

An indication of the impact of the cloud particles thermodynamic phase on the retrieval is shown in Fig. 7. In this case the libRadtran RTM was set with a "true" atmosphere characterized by a low-level cloud made of ice crystals and not water droplets. For the calculation of

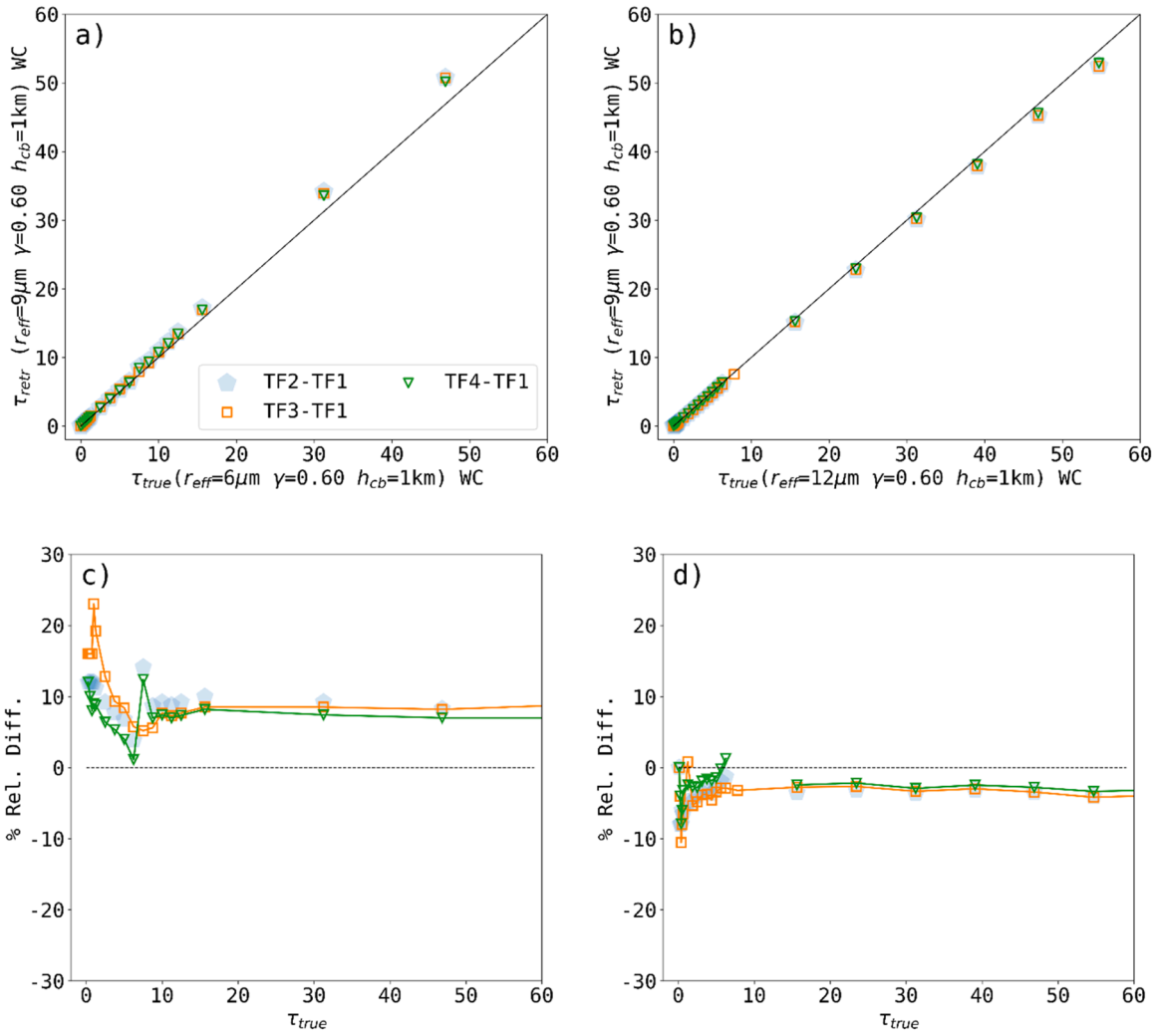


**Fig. 6.** Same as Fig. 4 but using modeled radiances with γ=0.60 and $r_{eff}$=6 μm (panels a and c) or $r_{eff}$=12 μm (panels b and d).

radiances, the libRadtran HEY parameterization [38,63], including complete scattering phase functions, was used together with a mixture of ice crystal shapes defined in the RTM as a general habit mixture [3]. Following the work of Grenfell and Warren [26] and Fitzpatrick et al. [[21], and references therein] on irradiance measurements, for transmittance computation purposes any ice crystal shape can be described as a collection of spheres with a $r_{eff}$ value such that the spheres have the same volume-to-area ratio as the crystal. We chose $r_{eff}$=20 μm, a size that can be considered representative of high-latitude, low-level ice clouds [59].

As discussed in the Introduction, Arctic low-level stratus clouds in late spring/summer are predominantly made of liquid droplets [28]. Therefore, even though in Fig. 7 we represent results obtained with a cloud made entirely of ice crystals, the low-level clouds we expect at THAAO are, at most, mixed-phase clouds with a small percentage of ice crystals. In particular, a realistic condition in late spring/summer is represented by a low-level mixed-phase cloud with ice crystals contributing about 10% to the total cloud water content. We can pretend that 1 layer out of 10 (10% of the total water content) is made of ice crystals and the remaining 9 layers contain liquid water. This layer is characterized by a τ that is generally at most 60% smaller (see Fig. 7b for τ<5 and τ>10) than a liquid water layer containing the same amount of water. From this simple argument, calculations suggest that if we ran the retrievals with the default assumption of a 100% liquid water cloud with $r_{eff}$=9 μm instead of a "true" cloud with a 10% contamination of ice crystals, we would incur in an overestimation of τ of less than 5% for most τ values. Worse results are visible in the small τ range between 5 and 8. As commented previously (see, e.g., Fig. 4), at the transition from thin to thick cloud regimes the two branches are close to one another and the retrievals can be less reliable.

## 4. Summary and conclusions

This work aims at assessing whether it is conceivable to estimate τ by means of continuous ground-based zenith radiance measurements in the UV-Vis-NIR range (320–950 nm) in the Polar environment. It does not validate a method to do so with actual measurements but investigates what conditions and ancillary measurements would be required in order to reach the goal. Such spectral zenith radiance observations have been performed at the Thule High Arctic Atmospheric Observatory (THAAO) since 2021, together with measurements of cloud base height (since 2019), broadband surface albedo (since 2016), and additional ancillary measurements.

Zenith radiance measurements at two different wavelengths from ground-based platforms are widely used to successfully estimate τ [10,11] by the NASA AERONET network. This technique can provide continuous estimates of τ, but it requires an environment with vegetated surfaces as the sharp difference in albedo at the two wavelengths used (440 nm and 870 nm) is a key element of the retrievals. The retrieval algorithms we use in this work are inspired by those available in the literature and partially replicate their formulations to build a set of transmissivity formulas. We test pairs of TFs to find a set that would, in

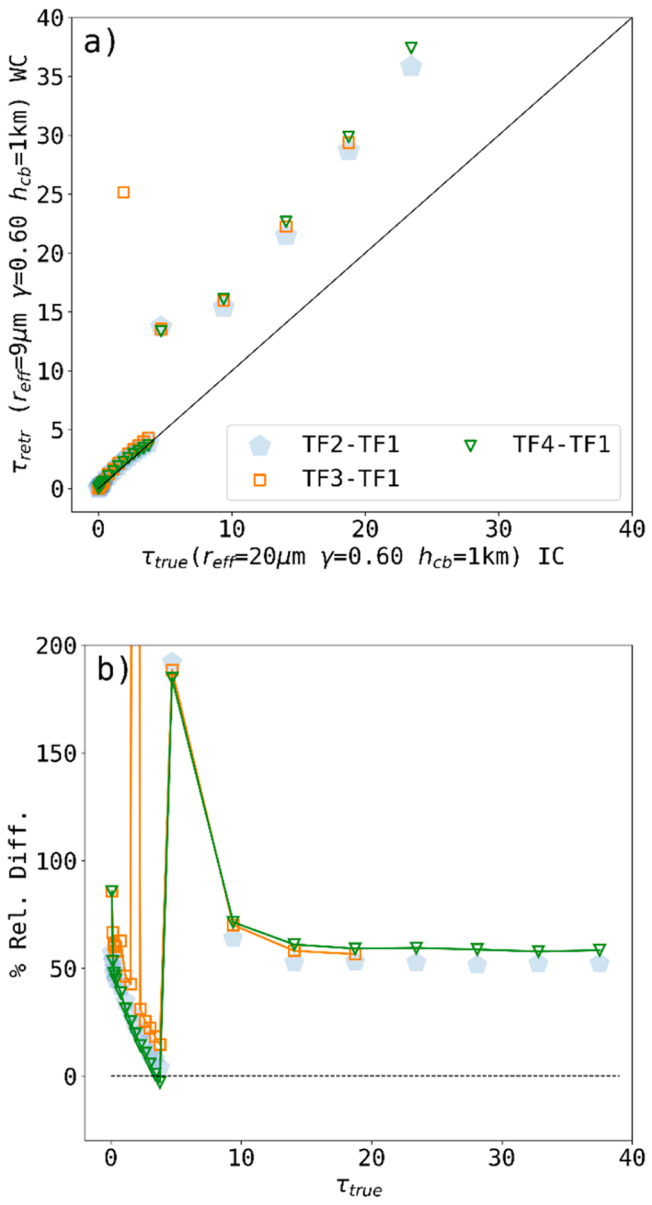


**Fig. 7.** Same as Fig. 4 but using modeled radiances with γ=0.60 and an ice cloud (IC) with $r_{eff}$=20 μm as "true" condition instead of a liquid water cloud.

principle, allow us to estimate τ univocally. The method's capability to obtain accurate cloud optical thickness estimates is focused on high albedo cases, which are challenging and poorly investigated. The model calculations rely on the libRadtran (v. 2.0.5) RTM package simulations. The impact of surface albedo (γ), cloud base height ($h_{cb}$), cloud effective radius ($r_{eff}$), cloud thermodynamic phase (ϕ), and solar zenith angle (θ) uncertainties on the various TFs used for τ retrievals is evaluated.

We test the chosen pairs of TFs by producing modeled radiances representing several different "true" atmospheric conditions and then retrieving τ imposing always the same default conditions (ϕ=water, θ=70°, γ=0.60, $h_{cb}$=1.0 km, $z_c$=500 m, and $r_{eff}$=9 μm). By doing this, we determine which ancillary information on the status of the atmosphere can be assumed and which have to be measured on-site. One of the most critical parameters is the surface albedo, and specifically the condition when only the broadband albedo is known (Fig. 4b), which is the case for the zenith UV-Vis-NIR radiance measurements at THAAO. In this case (modeled radiances are produced with a spectrally-resolved albedo $\gamma_{SP}$, but τ is retrieved using a broadband value), we find that not all the TFs pairs tested could be successfully used. TF2 vs. TF1 is unreliable for $\tau_{true}$>10 and fails above 20, whereas only TF4 vs. TF1 succeeds for very thick clouds (τ>30), showing an underestimation of approximately 5%. However, this pair is also the only one that requires the ancillary information on the cloud base height, which at THAAO is accurately provided by means of a ceilometer.

Tests also showed that a 50% error in $r_{eff}$ leads to approximately a 10% error in τ and that a 10% contamination of ice crystals in a predominantly low-level liquid water cloud leads to an error in determining τ estimated to be below 5%. All the tests showed that the most critical τ range is at the transition between thin and thick cloud regimes (generally from about 7 to 15), where the two regime branches are close to one another and the retrievals can be less reliable. All the sensitivity tests we conducted suggest that in the environmental conditions that characterize late spring and summer at THAAO, and given the observatory measurements capabilities, estimates of τ could be performed continuously and with good accuracy in high surface albedo conditions by means of zenith radiance measurements in the UV-Vis-NIR range. Based on the branches separation illustrated in Figs. 2 and 3 and the sensitivity test results of Figs. 4-7, we recommend the use of the TF3 vs. TF1 pair for τ values below 20 and the TF4 vs. TF1 combination for thicker clouds. Future work will apply these theoretical findings to actual radiance measurements and compare the obtained τ estimates with concurrent observations.

## Funding

This research has been supported by the Italian Antarctic Research Program (PNRA) through project PNRA18_00122 "CLouds And Radiation in the Arctic and Antarctica (CLARA2)" and by the Italian Arctic Research Programme (PRA) through project PRA2019-0009 "Effects of Changing Albedo and Precipitation on the Arctic Climate (ECAPAC)". Both PNRA and PRA are programs of the Ministry of University and Research.

The Italian activities at Thule High Arctic Atmospheric Observatory (THAAO) have been supported by the Istituto Nazionale di Geofisica e Vulcanologia (Environment Department) in the framework of the Multidisciplinary Analysis of Climate change indicators in the Mediterranean And Polar regions (MACMAP) project.

## CRediT authorship contribution statement

**Filippo Calì Quaglia:** Writing – review & editing, Writing – original draft, Visualization, Software, Methodology, Investigation, Formal analysis, Data curation, Conceptualization. **Giovanni Muscari:** Writing – review & editing, Writing – original draft, Supervision, Project administration, Methodology, Investigation, Funding acquisition, Conceptualization. **Daniela Meloni:** Writing – review & editing, Writing – original draft, Supervision, Methodology, Investigation, Conceptualization. **Annalisa Di Bernardino:** Writing – review & editing, Project administration. **Tatiana Di Iorio:** Writing – review & editing. **Giandomenico Pace:** Writing – review & editing, Project administration, Funding acquisition, Conceptualization. **Sebastian K. Schmidt:** Writing – review & editing, Supervision. **Alcide di Sarra:** Writing – review & editing, Writing – original draft, Supervision, Methodology, Investigation, Conceptualization.

## Declaration of competing interest

The authors declare that they have no known competing financial interests or personal relationships that could have appeared to influence the work reported in this paper.

## Data availability

The code for the retrievals is available upon request to the authors. The libRadtran model is freely available online (https://www.

libradtran.org/doku.php?id=download) and is run with different combinations, as described in detail in Section 2.3.

## Acknowledgments

We want to thank two anonymous reviewers for their valuable comments.

## Supplementary materials

Supplementary material associated with this article can be found, in the online version, at doi:10.1016/j.jqsrt.2024.109108.

## References

[1] Barnard JC, Long CN, Kassianov EI, McFarlane SA, Comstock JM, Freer M, McFarquhar GM. Development and evaluation of a simple algorithm to find cloud optical depth with emphasis on thin ice clouds. Open Atmospheric Sci J 2008;2(1):46–55. https://doi.org/10.2174/1874282300802010046.

[2] Barnard James C, Long CN. A simple empirical equation to calculate cloud optical thickness using shortwave broadband measurements. J Appl Meteorol 2004;43(7):1057–66. https://doi.org/10.1175/1520-0450(2004)043<1057:ASEETC>2.0.CO;2.

[3] Baum BA, Yang P, Heymsfield AJ, Platnick S, King MD, Hu Y-X, Bedka ST. Bulk Scattering Properties for the Remote Sensing of Ice Clouds. Part II: Narrowband Models. J Appl Meteorol 2005;44(12):1896–911. https://doi.org/10.1175/JAM2309.1.

[4] Bennartz R, Shupe MD, Turner DD, Walden VP, Steffen K, Cox CJ, et al. July 2012 Greenland melt extent enhanced by low-level liquid clouds. Nature 2013;496(7443):83–6. https://doi.org/10.1038/nature12002.

[5] Bierwirth E, Ehrlich A, Wendisch M, Gayet J-F, Gourbeyre C, Dupuy R, et al. Optical thickness and effective radius of Arctic boundary-layer clouds retrieved from airborne nadir and imaging spectrometry. Atmos Meas Tech 2013;6(5):1189–200. https://doi.org/10.5194/amt-6-1189-2013.

[6] Bintanja R, Krikken F. Magnitude and pattern of Arctic warming governed by the seasonality of radiative forcing. Sci Rep 2016;6(1):38287. https://doi.org/10.1038/srep38287.

[7] Brückner M, Pospichal B, Macke A, Wendisch M. A new multispectral cloud retrieval method for ship-based solar transmissivity measurements. J Geophys Res: Atmospheres 2014;119(19):11. https://doi.org/10.1002/2014JD021775. ,338-11,354.

[8] The impact of very high S/N spectroscopy on stellar physics: proceedings of the. In: Cayrel de Strobel R, editor. 132nd Symposium of the International Astronomical Union held in Paris, France, June 29-July 3, 1987. Dordrecht; Boston: Kluwer Academic Publishers; 1988.

[9] Ceppi P, Brient F, Zelinka MD, Hartmann DL. Cloud feedback mechanisms and their representation in global climate models. WIREs Climate Change 2017;8(4):e465. https://doi.org/10.1002/wcc.465.

[10] Chiu JC, Marshak A, Knyazikhin Y, Wiscombe WJ. Spectrally-invariant behavior of zenith radiance around cloud edges simulated by radiative transfer. Atmos Chem Phys 2010;10(22):11295–303. https://doi.org/10.5194/acp-10-11295-2010.

[11] Chiu JChristine, Marshak A, Knyazikhin Y, Wiscombe WJ, Barker HW, Barnard JC, Luo Y. Remote sensing of cloud properties using ground-based measurements of zenith radiance. J Geophys Res 2006;111(D16):D16201. https://doi.org/10.1029/2005JD006843.

[12] Chiu JC, Holmes JA, Hogan RJ, O'Connor EJ. The interdependence of continental warm cloud properties derived from unexploited solar background signals in ground-based lidar measurements. Atmos Chem Phys 2014;14(16):8389–401. https://doi.org/10.5194/acp-14-8389-2014.

[13] Coddington OM, Pilewskie P, Vukicevic T. The Shannon information content of hyperspectral shortwave cloud albedo measurements: quantification and practical applications. J Geophys Res: Atmospheres 2012;117(D4). https://doi.org/10.1029/2011JD016771.

[14] Curry JA, Ebert EE. Sensitivity of the thickness of arctic sea ice to the optical properties of clouds. Ann Glaciol 1990;14:43–6. https://doi.org/10.3189/S0260305500008235.

[15] Chylek P, Ramaswamy V. Simple approximation for infrared emissivity of water clouds. J Atmos Sci 1981.

[16] Dahlback A, Stamnes K. A new spherical model for computing the radiation field available for photolysis and heating at twilight. Planetary Space Sci 1991;39(5):671–83. https://doi.org/10.1016/0032-0633(91)90061-E.

[17] Di Biagio C, di Sarra A, Eriksen P, Ascanius SE, Muscari G, Holben B. Effect of surface albedo, water vapour, and atmospheric aerosols on the cloud-free shortwave radiative budget in the Arctic. Clim Dyn 2012;39(3–4):953–69. https://doi.org/10.1007/s00382-011-1280-1.

[18] Di Iorio T, di Sarra A, Pace G, Meloni D, Muscari G, Di Liberto L, et al. Cloud base height at the thule high arctic atmospheric observatory (THAAO_CBH). Agenzia Nazionale per le nuove tecnologie, l'energia e lo sviluppo economico sostenibile (ENEA); 2022. https://doi.org/10.13127/THAAO/CBH.

[19] Duncan BN, Ott LE, Abshire JB, Brucker L, Carroll ML, Carton J, et al. Space-based observations for understanding changes in the arctic-boreal zone. Rev Geophys 2020;58(1). https://doi.org/10.1029/2019RG000652.

[20] Emde C, Buras-Schnell R, Kylling A, Mayer B, Gasteiger J, Hamann U, et al. The libRadtran software package for radiative transfer calculations (version 2.0.1). Geosci Model Dev 2016;9(5):1647–72. https://doi.org/10.5194/gmd-9-1647-2016.

[21] Fitzpatrick MF, Brandt RE, Warren SG. Transmission of solar radiation by clouds over snow and ice surfaces: a parameterization in terms of optical depth, solar zenith angle, and surface albedo. J Climate 2004;17:266–75. https://doi.org/10.1175/1520-0442(2004)017<0266:TOSRBC>2.0.CO;2.

[22] Gallagher MR, Shupe MD, Miller NB. Impact of atmospheric circulation on temperature, clouds, and radiation at Summit Station, Greenland, with self-organizing maps. J Climate 2018;31(21):8895–915. https://doi.org/10.1175/JCLI-D-17-0893.1.

[23] Gardiner BG. Solar radiation transmitted to the ground through cloud in relation to surface albedo. J Geophys Res 1987;92(D4):4010. https://doi.org/10.1029/JD092iD04p04010.

[24] Gardner AS, Sharp MJ. A review of snow and ice albedo and the development of a new physically based broadband albedo parameterization. J Geophys Res 2010;115(F1):F01009. https://doi.org/10.1029/2009JF001444.

[25] Giles DM, Sinyuk A, Sorokin MG, Schafer JS, Smirnov A, Slutsker I, et al. Advancements in the Aerosol Robotic Network (AERONET) Version 3 database – automated near-real-time quality control algorithm with improved cloud screening for Sun photometer aerosol optical depth (AOD) measurements. Atmos Meas Tech 2019;12(1):169–209. https://doi.org/10.5194/amt-12-169-2019.

[26] Grenfell TC, Warren SG. Representation of a nonspherical ice particle by a collection of independent spheres for scattering and absorption of radiation. J Geophys Res: Atmospheres 1999;104(D24):31697–709. https://doi.org/10.1029/1999JD900496.

[27] Holben BN, Eck TF, Slutsker I, Tanré D, Buis JP, Setzer A, et al. AERONET—a federated instrument network and data archive for aerosol characterization. Remote Sens Environ 1998;66(1):1–16. https://doi.org/10.1016/S0034-4257(98)00031-5.

[28] Hu Y, Rodier S, Xu K, Sun W, Huang J, Lin B, Zhai P, Josset D. Occurrence, liquid water content, and fraction of supercooled water clouds from combined CALIOP/IIR/MODIS measurements. J Geophys Res: Atmospheres 2010;115(D4):2009JD012384. https://doi.org/10.1029/2009JD012384.

[29] Jung T, Gordon ND, Bauer P, Bromwich DH, Chevallier M, Day JJ, et al. Advancing polar prediction capabilities on daily to seasonal time scales. Bull Am Meteorol Soc 2016;97(9):1631–47. https://doi.org/10.1175/BAMS-D-14-00246.1.

[30] Khatri P, Iwabuchi H, Hayasaka T, Irie H, Takamura T, Yamazaki A, et al. Retrieval of cloud properties from spectral zenith radiances observed by sky radiometers. Atmos Meas Tech 2019;12(11):6037–47. https://doi.org/10.5194/amt-12-6037-2019.

[31] Kikuchi N, Nakajima T, Kumagai H, Kuroiwa H, Kamei A, Nakamura R, Nakajima TY. Cloud optical thickness and effective particle radius derived from transmitted solar radiation measurements: Comparison with cloud radar observations. J Geophys Res 2006;111(D7):D07205. https://doi.org/10.1029/2005JD006363.

[32] King MD, Platnick S, Yang P, Arnold GT, Gray MA, Riedi JC, et al. Remote sensing of liquid water and ice cloud optical thickness and effective radius in the arctic: application of airborne multispectral MAS data. J Atmos Ocean Technol 2004;21(6):857–75. https://doi.org/10.1175/1520-0426(2004)021<0857:RSOLWA>2.0.CO;2.

[33] Kurucz RL. Synthetic Infrared Spectra. In: Presented at the Infrared Solar Physics. 154; 1994. p. 523.

[34] LeBlanc SE, Pilewskie P, Schmidt KS, Coddington OM. A spectral method for discriminating thermodynamic phase and retrieving cloud optical thickness and effective radius using transmitted solar radiance spectra. Atmos Meas Tech 2015;8(3):1361–83. https://doi.org/10.5194/amt-8-1361-2015.

[35] Leontyeva E, Stamnes K. Estimations of cloud optical thickness from ground-based measurements of incoming solar radiation in the arctic. J Climate 1994;7(4):566–78. https://doi.org/10.1175/1520-0442(1994)007<0566:EOCOTF>2.0.CO;2.

[36] Marshak A, Knyazikhin Y, Davis AB, Wiscombe WJ, Pilewskie P. Cloud-vegetation interaction: Use of normalized difference cloud index for estimation of cloud optical thickness. Geophys Res Lett 2000;27(12):1695–8. https://doi.org/10.1029/1999GL010993.

[37] Marshak Alexander, Knyazikhin Y, Evans KD, Wiscombe WJ. The "RED versus NIR" plane to retrieve broken-cloud optical depth from ground-based measurements. J Atmos Sci 2004;61(15):1911–25. https://doi.org/10.1175/1520-0469(2004)061<1911:TRVNPT>2.0.CO;2.

[38] Mayer B, Kylling A. Technical note: the libRadtran software package for radiative transfer calculations—description and examples of use. Atmos Chem Phys 2005;5(7):1855–77. https://doi.org/10.5194/acp-5-1855-2005.

[39] McBride PJ, Schmidt KS, Pilewskie P, Kittelman AS, Wolfe DE. A spectral method for retrieving cloud optical thickness and effective radius from surface-based transmittance measurements. Atmos Chem Phys 2011;11(14):7235–52. https://doi.org/10.5194/acp-11-7235-2011.

[40] Meloni D, Calì Quaglia F, Ciardini V, Di Bernardino A, Di Iorio T, Iaccarino A, Muscari G, Pace G, Scarchilli C, di Sarra A. Shortwave and longwave components of the surface radiation budget measured at the thule high arctic atmospheric observatory, Northern Greenland. Earth Syst Sci Data 2024;16(1):543–66. https://doi.org/10.5194/essd-16-543-2024.

[41] Meloni D, di Sarra A, Di Iorio T, Pace G, Muscari G, Iaccarino A, Calì Quaglia F. Downward shortwave irradiance at the thule high arctic atmospheric observatory (THAAO_DSI). a. Agenzia Nazionale per le nuove tecnologie, l'energia e lo sviluppo economico sostenibile (ENEA); 2022. https://doi.org/10.13127/THAAO/DSI.
[42] Meloni D, di Sarra A, Di Iorio T, Pace G, Muscari G, Iaccarino A, Calì Quaglia F. Upward shortwave irradiance at the thule high arctic atmospheric observatory (THAAO_USI). b. Agenzia Nazionale per le nuove tecnologie, l'energia e lo sviluppo economico sostenibile (ENEA); 2022. https://doi.org/10.13127/THAAO/USI.
[43] Min Q, Harrison LC. Cloud properties derived from surface MFRSR measurements and comparison with GOES results at the ARM SGP Site. Geophys Res Lett 1996;23 (13):1641–4. https://doi.org/10.1029/96GL01488.
[44] Nakajima T, King MD. Determination of the optical thickness and effective particle radius of clouds from reflected solar radiation measurements. Part I: theory. J Atmos Sci 1990;47(15):1878–93. https://doi.org/10.1175/1520-0469(1990)047<1878:DOTOTA>2.0.CO;2.
[45] Niple ER, Scott HE, Conant JA, Jones SH, Iannarilli FJ, Pereira WE. Application of oxygen A-band equivalent width to disambiguate downwelling radiances for cloud optical depth measurement. Atmos Meas Tech 2016;9(9):4167–79. https://doi.org/10.5194/amt-9-4167-2016.
[46] Norgren MS, Wood J, Schmidt KS, van Diedenhoven B, Stamnes SA, Ziemba LD, et al. Above-aircraft cirrus cloud and aerosol optical depth from hyperspectral irradiances measured by a total-diffuse radiometer. Atmos Meas Tech 2022;15(5): 1373–94. https://doi.org/10.5194/amt-15-1373-2022.
[47] Peng Y, Lohmann U, Leaitch R, Banic C, Couture M. The cloud albedo-cloud droplet effective radius relationship for clean and polluted clouds from race and fire.ace: evidence for indirect aerosol effect. J Geophys Res: Atmospheres 2002;107(D11). https://doi.org/10.1029/2000JD000281. AAC 1-1-AAC 1-6.
[48] Platnick S, Li JY, King MD, Gerber H, Hobbs PV. A solar reflectance method for retrieving the optical thickness and droplet size of liquid water clouds over snow and ice surfaces. J Geophys Res: Atmospheres 2001;106(D14):15185–99. https://doi.org/10.1029/2000JD900441.
[49] Quaas J, Arola A, Cairns B, Christensen M, Deneke H, Ekman AML, et al. Constraining the Twomey effect from satellite observations: issues and perspectives. Atmos Chem Phys 2020;20(23):15079–99. https://doi.org/10.5194/acp-20-15079-2020.
[50] Rantanen M, Karpechko AYu, Lipponen A, Nordling K, Hyvärinen O, Ruosteenoja K, et al. The Arctic has warmed nearly four times faster than the globe since 1979. Commun Earth Environ 2022;3(1):168. https://doi.org/10.1038/s43247-022-00498-3.
[51] Schmidt S, Boisvert-McPartland L, Taylor P, Bucholtz A, Cesana G, DeMott P, et al. Arctic radiation-cloud-aerosol-surface interaction experiment. ARCSIX; 2021. p. 40.
[52] Shettle EP. Models of aerosols, clouds, and precipitation for atmospheric propagation studies. AGARD; 1990.
[53] Shupe MD. Clouds at arctic atmospheric observatories. Part II: thermodynamic phase characteristics. J Appl MeteorolJ Appl Meteorol Climatol 2011;50(3): 645–61. https://doi.org/10.1175/2010JAMC2468.1.
[54] Shupe MD, Rex M, Blomquist B, Persson POG, Schmale J, Uttal T, et al. Overview of the MOSAiC expedition: atmosphere. Elementa: Sci Anthropocene 2022;10(1): 00060. https://doi.org/10.1525/elementa.2021.00060.
[55] Stamnes K, Tsay S-C, Wiscombe W, Jayaweera K. Numerically stable algorithm for discrete-ordinate-method radiative transfer in multiple scattering and emitting layered media. Appl Opt 1988;27(12):2502. https://doi.org/10.1364/AO.27.002502.
[56] Sinyuk A, Holben BN, Eck TF, Giles DM, Slutsker I, Korkin S, Schafer JS, Smirnov A, Sorokin M, Lyapustin A. The AERONET Version 3 aerosol retrieval algorithm, associated uncertainties and comparisons to Version 2. Atmos Meas Tech 2020;13 (6):3375–411. https://doi.org/10.5194/amt-13-3375-2020.
[57] Twomey S. The Influence of Pollution on the Shortwave Albedo of Clouds. J Atmos Sci 1977;34(7):1149–52. https://doi.org/10.1175/1520-0469(1977)034<1149:TIOPOT>2.0.CO;2.
[58] Uttal T, Army US, Hampshire N, City Q. Surface Heat Budget of the Arctic Ocean. Bull Am Meteorol Soc 2002;83(2):255–76. https://doi.org/10.1175/1520-0477(2002)083<0255:SHBOTA>2.3.CO;2.
[59] van Diedenhoven B, Ackerman AS, Fridlind AM, Cairns B, Riedi J. Global statistics of ice microphysical and optical properties at tops of optically thick ice clouds. J Geophys Res: Atmospheres 2020;125:e2019JD031811. https://doi.org/10.1029/2019JD031811.
[60] Voigt A, Albern N, Ceppi P, Grise K, Li Y, Medeiros B. Clouds, radiation, and atmospheric circulation in the present-day climate and under climate change. WIREs Climate Change 2021;12(2). https://doi.org/10.1002/wcc.694.
[61] Wendisch M, Brückner M, Crewell S, Ehrlich A, Notholt J, Lüpkes C, et al. Atmospheric and surface processes, and feedback mechanisms determining arctic amplification: a review of first results and prospects of the (AC)3 project. Bull Am Meteorol Soc 2023;104(1):E208–42. https://doi.org/10.1175/BAMS-D-21-0218.1.
[62] Wood R, Hartmann DL. Spatial variability of liquid water path in marine low cloud: the importance of mesoscale cellular convection. Journal of Climate 2006;19(9): 1748–64. https://doi.org/10.1175/JCLI3702.1.
[63] Yang Ping, Liou KN, Wyser Klaus, Mitchell David. Parameterization of the scattering and absorption properties of individual ice crystals. J Geophys Res: Atmospheres 2000;105(D4):4699–718. https://doi.org/10.1029/1999JD900755.
[64] Yin B, Min Q. Climatology of aerosol and cloud optical properties at the atmospheric radiation measurements climate research facility barrow and atqasuk sites. J Geophys Res: Atmospheres 2014;119(4):1820–34. https://doi.org/10.1002/2013JD020296.
[65] Zhou Y, Yang Y, Gao M, Zhai P-W. Cloud detection over snow and ice with oxygen A- and B-band observations from the Earth Polychromatic Imaging Camera (EPIC). Atmos Meas Tech 2020;13(3):1575–91. https://doi.org/10.5194/amt-13-1575-2020.
[66] Zibordi G, Ruddick K, Ansko I, Moore G, Kratzer S, Icely J, Reinart A. In situ determination of the remote sensing reflectance: an inter-comparison. Ocean Sci 2012;8(4):567–86. https://doi.org/10.5194/os-8-567-2012.
[67] Zinner T, Hausmann P, Ewald F, Bugliaro L, Emde C, Mayer B. Ground-based imaging remote sensing of ice clouds: uncertainties caused by sensor, method and atmosphere. Atmos Meas Tech 2016;9(9):4615–32. https://doi.org/10.5194/amt-9-4615-2016.
[68] Zinner T, Schwarz U, Kölling T, Ewald F, Jäkel E, Mayer B, Wendisch M. Cloud geometry from oxygen-A-band observations through an aircraft side window. Atmos Meas Tech 2019;12(2):1167–81. https://doi.org/10.5194/amt-12-1167-2019.